A Causal Regularizing Deconvolution Filter for Optimal Waveform Reconstruction

Nicholas G. Paulter, Jr.

Abstract—A causal regularizing filter is described for selecting an optimal reconstruction of a signal from a deconvolution of its measured data and the measurement instrument's impulse response. Measurement noise and uncertainties in the instrument's response can cause the deconvolution (or inverse problem) to be ill-posed, thereby precluding accurate signal restoration. Nevertheless, close approximations to the signal may be obtained by using reconstruction techniques that alter the problem so that it becomes numerically solvable. A regularizing reconstruction technique is implemented that automatically selects the optimal reconstruction via an adjustable parameter and a specific stopping criterion, which is also described. Waveforms reconstructed using this filter do not exhibit large oscillations near transients as observed in other regularized reconstructions. Furthermore, convergence to the optimal solution is rapid.

I. INTRODUCTION

THE DATA ACQUIRED from the measurement of a signal is affected by the measuring instrument and, therefore, can be described by the convolution of the signal with the instrument's impulse response. In particular, discrete measured data can be described by the discrete convolution equation

$$f_r = \sum_{m=0}^{N-1} g_m h'_{\tau-m} + n_\tau \equiv g_\tau^* h'_\tau + n_\tau, \quad 0 \leq \Gamma \leq 2N-1. \tag{1}$$

Please see the Appendix for a description of all variables used in this paper. The discrete frequency-domain representation of (1) is

$$F_k = G_k H'_k + N_k, \quad 0 \leq k \leq 2N-1. \tag{2}$$

It is necessary to remove the effects of the measurement instrument from the data to obtain an accurate representation of the signal. This is accomplished through a reconstruction, the first step of which is a discrete Fourier transform (DFT) of the waveforms, the second a deconvolution (division of spectra), and lastly an inverse DFT. The deconvolution is given by

$$G_k = \frac{F_k - N_k}{H'_k}. \tag{3}$$

A subsequent inverse DFT of (3) yields gm, the discretized replica of the input signal. Because only an approximation

to H'_k is known and N_k is not known, G_k cannot be found. Therefore, only an approximate solution to this "blind" deconvolution [1] can be found,

$$G''_k = \frac{F_k}{H_k}, \tag{4}$$

where H_k is an approximation to H_k and is never zero. Because of the lack of knowledge on N_k and H'_k, H_k must be varied to get the "best" solution. However, a more suitable approach is not to vary H_k, but to introduce another function, a regularizing filter, that can be easily varied. The iterative solution is then given by

$$G_k \approx G'_k = G''_k R_k \tag{5}$$

where R_k is the causal regularizing filter that has an integral optimizing parameter. The R_k is developed here.

Iterative techniques for solving the ill-posed or blind deconvolution problem have been studied extensively (for examples, see [2]–[10]). In particular, regularized iterative techniques are frequently used for this purpose (for examples, see [11]–[17]). Biemond and his coauthors provide an overview of iterative image (2-D signal) reconstruction as applied to photographic images, [18] the concepts of which can be easily applied to the reconstruction of one-dimensional signals. A good development of the regularization process in image restoration is given by Ross [19].

The reconstruction technique described here uses a regularizing operator similar to that developed by Tikhonov and Arsenin for solving ill-posed problems [20]. The magnitude of the regularizing filter is developed in Section II, the stopping criterion and errors in Section III, and the phase of the regularizing filter in Section IV. Results of this reconstruction are presented in Section V. The waveforms used consist of real-valued discrete data representing step or impulse-like pulses.

II. REGULARIZING FILTER

The criteria for the regularizing filter are the error

$$E_k = G_k - G'_k = \frac{F_k - N_k}{H_k + A'_k} - \frac{F_k R_k}{H_k} \tag{6}$$

and its derivative with respect to H_k

$$\frac{dE_k}{dH_k} = \frac{d(F_k - N_k)}{H_k + A'_k} - \frac{F_k - N_k}{(H_k + A'_k)^2}\left[1 + \frac{dA'_k}{dH_k}\right]$$
$$+ \frac{F_k R_k}{H_k^2} - \frac{F_k}{H_k}\frac{dR_k}{dH_k} - \frac{R_k}{H_k}\frac{dF_k}{dH_k} \tag{7}$$

equal zero, where $A'_k = (H'_k - H_k)$. The H'_k is unknown so that only an approximation to A'_k, A_k, will be used. Equation (7) can be simplified using the following assertions: (a) $dN_k/dH_k = 0$, (b) $dR_k/dH_k = 0$ because R_k will not vary with H_k for a given reconstruction, (c) $dA'_k/dH_k \approx 0$ for $H'_k \approx H_k$, and (d) the quantity $[1/(H_k + A'_k) - R_k/H_k] \approx 0$ for $N_k < F_k$ and small A'_k. Using these assertions in (7), setting (7) to zero, and solving for R_k gives

$$R_k = \left[\frac{F_k - N_k}{F_k}\right] \frac{H_k^2}{(H_k + A_k)^2}. \quad (8)$$

Another solution for R_k comes from setting (6) to zero:

$$R_k = \left[\frac{F_k - N_k}{F_k}\right]\left[\frac{H_k}{H_k + A_k}\right]. \quad (9)$$

Because (8) and (9) are not equal, (8), (9), or their combination must be used to represent R_k. Furthermore, approximations to (8) and (9) will be used to obtain the regularization filter because N_k is unknown and $H_k = -A_k$ will cause instabilities in G'_k. These approximations to (8) and (9) will not contain any phase information (examined in Section V) and are given by

$$R_{1,k} = \frac{|H_k|}{|H_k| + |A_k|}$$

$$R_{2,k} = \frac{|H_k|^2}{|H_k|^2 + 2|H_k A_k| + |A_k|^2}$$

$$R_{3,k} = \frac{|H_k|^2}{|H_k|^2 + |A_k|^2}. \quad (10)$$

Other approximations are possible but they can be easily ruled out, as can be $R_{2,k}$ which was maintained to illustrate how the other possible filters were ruled out. To select which of the functions in (10) will provide the optimal reconstruction, compare the differences of the errors between a regularized solution and a target solution:

$$E_k = \left[T_k - \frac{|F_k|}{|H_k|}R_{i,k}\right]^2 - \left[T_k - \frac{|F_k|}{|H_k|}R_{j,k}\right]^2;$$
$$i, j = 1, 2, 3; i \neq j; \quad (11)$$

where T_k is a target solution $|F_k|/|H_k|, |F_k|/|H_k + A_k|$, or $|F_k - N_k|/|H_k + A_k|$; $|F_k|/|H_k|$ being the least realistic and $|F_k - N_k|/|H_k + A_k|$ the most realistic. Using (11) it can be shown that the errors associated with $R_{2,k}$-regularized solutions are greater than those for $R_{1,k}$- and $R_{3,k}$- regularized solutions for the target solutions $|F_k|/|H_k|$ and $|F_k|/|H_k + A_k|$ for all k. No such result arises using the target $|F_k - N_k|/|H_k + A_k|$ because the sign of E_k is N_k-dependent. However, one can rule out $R_{2,k}$ as a possible filter based on the comparison using targets $|F_k|/|H_k|$ and $|F_k|/|H_k + A_k|$. The sign of E_k using $R_{1,k}$- and $R_{3,k}$-regularized solutions exhibits a k-dependence for all target solutions. Consequently, it is necessary to determine the form of A_k and the bounds on the regularizing filter before a possible selection can be made.

The bounds on R_k are $0 < |R_k| < 1$. The strict inequalities are necessary because (a) the search is for an approximate solution and $|R_k| = 1$ implies $|H'_k|$ is known exactly, and (b) $|R_k| = 0$ is not of interest. Furthermore,

it can be assumed that the deconvolution errors are primarily in the high-frequency end of the spectrum where N_k and uncertainties in H_k have the greatest effect. This assumption was also made by others [21] who, in their work, separated the spectrum into two parts, one containing primarily "information" and the other primarily "noise." That separation was based on the bandwidth of the bandlimiting element in the measurement circuit. In an example, they used an information band of dc to 80 GHz for a 40-GHz test-device bandwidth [8]. Their filter attempted to control the magnitude of the noise without significantly affecting the information portion by keeping the standard deviation of the rms frequency error (defined therein as the difference between the iterative result and spectral division) over the information band small [8].

To preferentially attenuate the high-frequency components, $|R_k|$ should be a decreasing function of k. Also, $|R_k|$ should vary smoothly to avoid ringing. Further insight into the form of A_k can be obtained by rewriting (5) and considering only its magnitude with, as an example, $|R_k| = R_{1,k}$:

$$|G'_k| = \frac{|F_k|}{|H_k|}\frac{|H_k|}{|H_k| + |A_k|} = \frac{|F_k|}{|H_k|}\frac{|F_k|}{|F_k| + |A_k G'_k|}. \quad (12)$$

The $A_k G''_k$ is the DFT of two convolved time-domain functions, and its magnitude must increase with k so that $|R_k|$ decreases with k. These requirements can be satisfied by A_k being the DFT of a difference operator

$$|A_k| = \alpha|D_{k,j}| \quad (13)$$

where α is the adjustable parameter of the regularizing filter and $D_{k,j}$ is the spectrum of the jth-order difference operator $(j = 1, 2, 3, \ldots)$. For examples, the first two difference operators are: $d_{m,1} = \{1, -1, 0, \ldots\}$ and $d_{m,2} = \{1, -2, 1, 0 \ldots\}$. Because of the bounds placed on $|R_k|$, the limits on α are $0 < \alpha < \infty$. To select the optimal order, compare, for example, $R_{k,1}$-regularized solutions to the target $|F_k|/|H_k|$:

$$E_{k,j} = \left|\frac{F_k}{H_k}\right|^2\left[1 - \frac{|H_k|}{|H_k| + \alpha|D_{k,j}|}\right]^2$$
$$= \left|\frac{F_k}{H_k}\right|^2\left[\frac{\alpha|D_{k,1}|^j}{|H_k| + \alpha|D_{k,1}|^j}\right]^2. \quad (14)$$

The $|D_{k,j}| = |D_{k,1}|^j$ and $|D_{k,1}| = [2 - 2\cos(2\pi k/2N)]^1/2$, so that $0 \leq |D_{k,1}| < 1$ for $0 \leq k < N/3, |D_{k,1}| = 1$ for $k = N/3$, and $|D_{k,1}| > 1$ for $N/3 < k \leq N$. A comparison of the ratios of (14) for j and $j + 1$ and for $k > N/3$, where it is already assumed the majority of deconvolution errors resides and where $|R_k|$ has the greatest effect, shows that $E_{k,j} < E_{k,j+1}$. Accordingly, choose $j = 1$ and set $A_k = \alpha D_{k,1}$. Experiments support this choice in that any ringing observed in g'_m increases with j.

This A_k, however, does not help in choosing between $R_{1,k}$ or $R_{3,k}$. Using either one in waveform reconstructions did not provide consistent results in that failure of $R_{1,k}$ or $R_{3,k}$ was not predictable. However, if one filter failed, the other provided a good solution (minimal amount of unrealistic oscillations). Consequently, it was decided to use both filters with weights, $w_{1,\alpha}$ for $R_{k,1}$ and $w_{3,\alpha}$

for $R_{k,3}$, and an appropriate weighting criterion. The weights should vary only with α because a variation in k describes a new filter. To determine the weights consider the difference between $R_{k,1}$- and $R_{k,3}$-regularized reconstructions:

$$E_\alpha = \sum_k \left[\frac{|F_k|}{|H_k|} \frac{|H_k|^2}{|H_k|^2 + \alpha^2 |D_{k,1}|^2} - \frac{|F_k|}{|H_k|} \frac{|H_k|}{|H_k| + \alpha |D_{k,1}|} \right]$$

$$= \sum_k \frac{\alpha |F_k|}{(|H_k|\alpha|D_{k,1}|)(|H_k|^2 + \alpha^2 |D_{k,1}|^2)}$$

$$\times (|H_k||D_{k,1}| - \alpha |D_{k,1}|^2)$$

$$= C_\alpha \sum_k (|H_k||D_{k,1}| - \alpha |D_{k,1}|^2) = C_\alpha Y_\alpha \qquad (15)$$

where Y_α will be used to determine the weights. The weighting criteria are: (a) $w_{1,\alpha} = w_{3,\alpha}$ for $Y_\alpha = 0$ because $R_{1,k}$ and $R_{3,k}$ are equally valid, (b) $w_{1,\alpha}$ is a minimum when Y_α is a maximum because $R_{3,k}$ would be preferred, and (c) $w_{1,\alpha} + w_{3,\alpha} = 1$. The weights are then

$$w_{1,\alpha} = \frac{1}{2} \left[1 - \frac{Y_\alpha}{Y_{\alpha,\max} - Y_{\alpha,\lim}} \right]$$

$$w_{3,\alpha} = 1 - w_{1,\alpha} \qquad (16)$$

where $Y_{\alpha,\lim}$ is the value of Y_α when α is so large that the computer result of $|D_{k,1}||H_k| - \alpha|D_{k,1}|^2$ is $-\alpha|D_k, 1|^2$. The weight $w_{1,\alpha}$ is set to 1 for $Y_\alpha \leq Y_{\alpha,\lim}$. Other weighting schemes may be used; however, this is straightforward and works well (see Section V). Using these weights, the magnitude of the reconstructed spectrum becomes

$$|G'_k(\alpha)| = \frac{|F_k|}{|H_k|} (w_{1,\alpha} R_{1,k} + w_{3,\alpha} R_{3,k}) = \frac{|F_k|}{|H_k|} |R_k|. \quad (17)$$

III. STOPPING CRITERION AND ERRORS

The stopping criterion for the iterative reconstruction (17) is examined. Using (10) and (13) in (17) it can be shown that

$$|G'_k(\alpha)| \geq |G'_k(\alpha + \delta)| \qquad (18)$$

for all k, where δ is a positive increment, so that

$$\frac{\partial |G'_k(\alpha)|}{\partial \alpha} \leq 0. \qquad (19)$$

Adding the contributions of (19) for all k gives the total change in the magnitude of the reconstructed spectrum:

$$\Gamma_\alpha = \sum_{k=0}^{N-1} \frac{\partial |G'_k(\alpha)|}{\partial \alpha} \leq 0. \qquad (20)$$

A stable and optimal solution is found when τ_α, the optimizing functional, exhibits a maximum; this is where the spectrum is
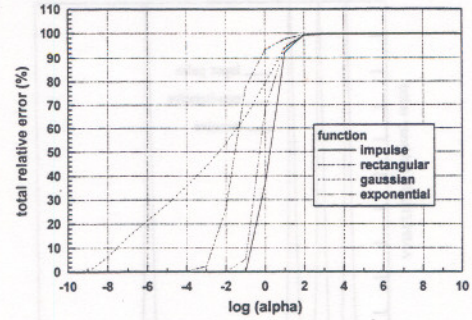

Fig. 1. Total relative error for $H_k = H'_k$ = DFT of a Gaussian, exponential, rectangular, or impulse function.

the most stable to changes in α. This value of α is the optimal stopping criterion and is designated α_0.

The relative errors for the proposed technique are

$$E_{R,K} = \frac{|G_k| - |G'_k|}{|G_k|}$$

$$= 1 - \frac{|H'_k|}{|H_k|} \left[W_{1,\alpha} \frac{|H_k|}{|H_k| + \alpha_0 |D_{k,1}|} \right.$$

$$\left. + w_{3,\alpha} \frac{|H_k|^2}{|H_k|^2 + \alpha_0^2 |D_{k,1}|^2} \right]. \qquad (21)$$

To analyze the error let $H_k = H'_k$ and then (21) becomes (22) at the bottom of the page.

Fig. 1 displays the total relative error, $\sum_k E_{R,k}^2$, as a function of α_0 for $H_k = H'_k$ equal to the DFT of a Gaussian, $e^{-[m-25]^2/9}$; an exponential, $e^{-[m-1]/2}$; a delta, $\delta[m-1]$; or a rectangular pulse, $u[m - 51] - u[m - 100]$. For $H_k = H'_k$ being an exponential or delta, $\alpha_0 \leq 10^{-3}$, and the total relative error was less than 0.01%. When $H_k = H'_k$ is a rectangular pulse, $\alpha_0 \leq 10^{-20}$. Because this value of α_0 provides virtually no filtering, α_0 is set to zero, $E_{R,k}$ goes to zero, and the reconstruction result is accurate (Fig. 2(a)). When $H_k = H'_k$ is Gaussian, the reconstruction errors can be large (Fig. 2(b)).

IV. PHASE

The $|R_k|$ is a magnitude-only function and, therefore, is not physically realistic unless a causal phase function can be associated with it; that is, $R_k = |R_k| \exp(i\theta_k)$, where θ_k is the phase of R_k. If R_k is also a minimum phase function, then θ_k can be found from R_k through the Hilbert transform. [22] The first step is to determine if $|R_k|$ is square-summable,

$$\sum_k |R_k|^2 \leq \infty \qquad (23)$$

$$E_{R,K} = \alpha_0 |D_{k,1}| \times \frac{w_{1,\alpha} |H_k|(|H_k| - \alpha_0 |D_{k,1}|) + \alpha_0 |D_{k,1}|(|H_k| + \alpha_0 |D_{k,1}|)}{(|H_k| + \alpha_0 |D_{k,1}|)(|H_k|^2 + \alpha_0^2 |D_{k,1}|^2)}. \qquad (22)$$
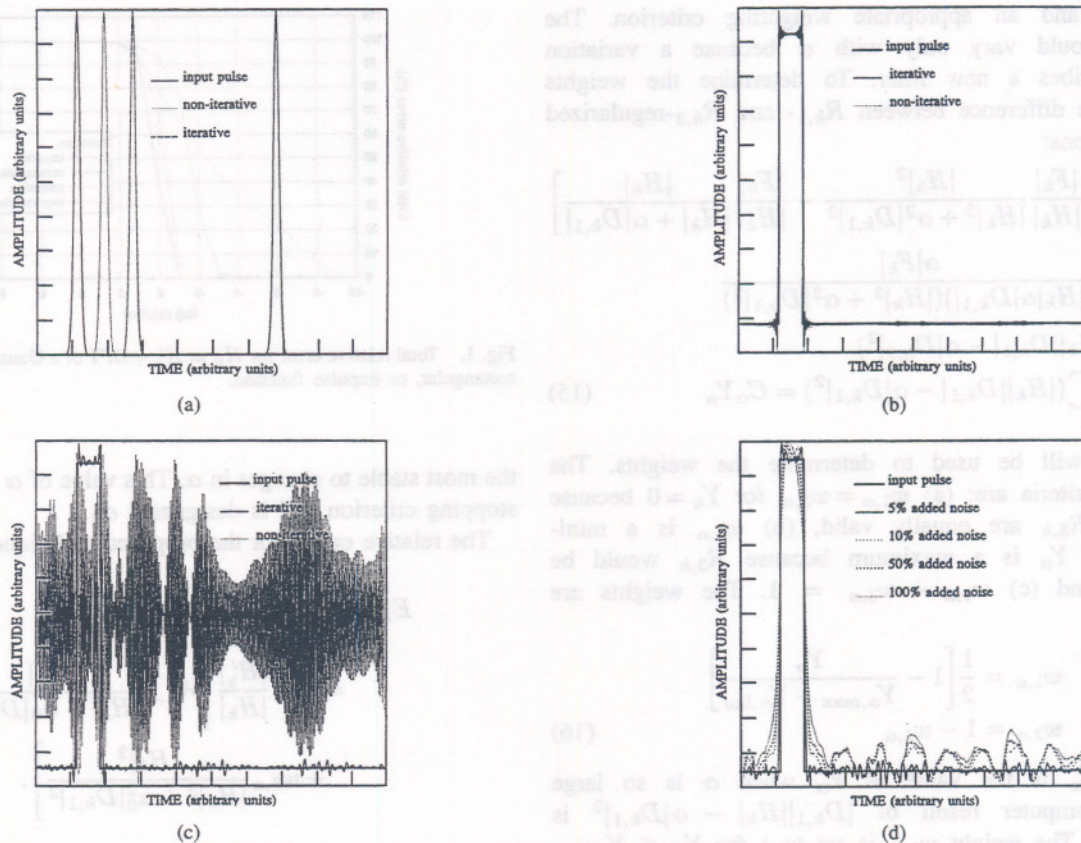
(a)

(b)

(c)

(d)

Fig. 2. Reconstruction of analytic waveforms with and without N_k. The plots in (a) show the result of the iterative process and spectral division (SD) on the reconstruction of a Gaussian pulse from a convolution of the same Gaussian and a rectangular pulse. The time shift is artificial. The far right trace is an overlay of the three traces shown to its left. The curves in (b) display the iterative and SD reconstructions of a square pulse. The target rectangular pulse is also shown. The curves in (c) are similar to those in (b) except that 1% zero-mean noise was added to the convolved waveform. (See text for an explanation of this percentage.) The traces in (d) show the results of the iterative reconstruction using 5%, 10%, 50%, and 100% additive zero-mean noise.

and if it is, then its DFT exists. Because $|R_k| \leq 1$ for all k and $|R_k|$ becomes vanishingly small at $k = N$, $|R_k|$ is square-summable. Next, $|R_k|$ must be shown to be the magnitude of the DFT of a causal function. This is established using the Paley–Wiener criterion [23], which states that if a function is bandlimited or if there are any regions over which it is zero then it cannot be the Fourier transform of a causal function. Since $0 < |R_k| \leq 1$ for all k, it is not bandlimited, and there are no regions over which it is zero; therefore, $|R_k|$ is the DFT of a causal function. Consequently, there exists some m_0 such that r_m, the time-domain representation of R_k, is zero for $m \leq m_0$.

To determine the phase of R_k, note that R_k can be described by three parts: (a) the minimum phase, (b) the all-pass principal, and (c) the all-pass linear parts [24]. Parts (b) and (c) both have unit magnitude and, consequently, do not affect $|R_k|$. Therefore, R_k is defined to be a minimum phase function and θ_k is obtained from $|R_k|$ through the Hilbert transform.

V. RESULTS

The results of using a causal regularizing filter, R_k, in reconstructions are presented here. Section V-A contains the results of the iterative reconstruction of waveforms described by analytic functions. Also, a comparison to the SD of F_k by

H_k is made and the effects of N_k are examined. Section V-B displays the results of two reconstructions and the associated stopping criterion curves. Lastly, selected statistics of pulse parameters describing 59 reconstructions are presented and compared to the method indicated in [17]. This number of reconstructions is taken from an arbitrary selection of waveform pairs.

A. Reconstruction of Analytic Waveforms Involving Gaussian Waveforms

The results of the iterative and SD reconstruction of a Gaussian pulse from the convolution of the same Gaussian with a square pulse are shown in Fig. 2(a). The calculated 10–90% and 20–80% rise times, for the input Gaussian, the iterative result, and the SD result are identical. Fig. 2(b) shows the results of the reconstruction of the square pulse for the iterative technique and the SD. In Fig. 2(c), the reconstructions of the square pulse for the iterative technique and SD are presented where 1% n_m has been added to the convolved waveform. Fig. 2(d) shows the results of the effect of 5, 10, 50, and 100% n_m on the iterative technique. These percentages are given as the ratio of the peak-to-peak noise amplitude to that of the convolved waveform. The noise was generated using a pseudo-random number generator.
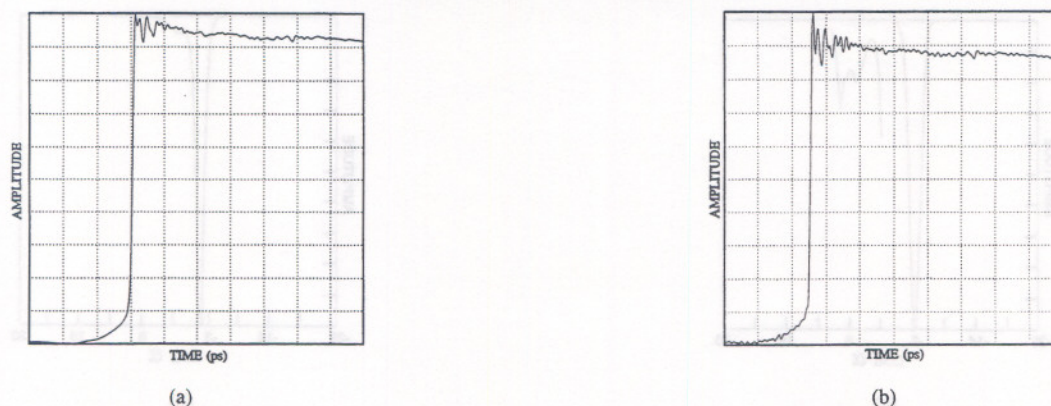
(a)

(b)

Fig. 3.   Reconstruction of real data using an approximate system response (Gaussian). The plots in (a) and (b) correspond to the measured data and reconstruction result, respectively.
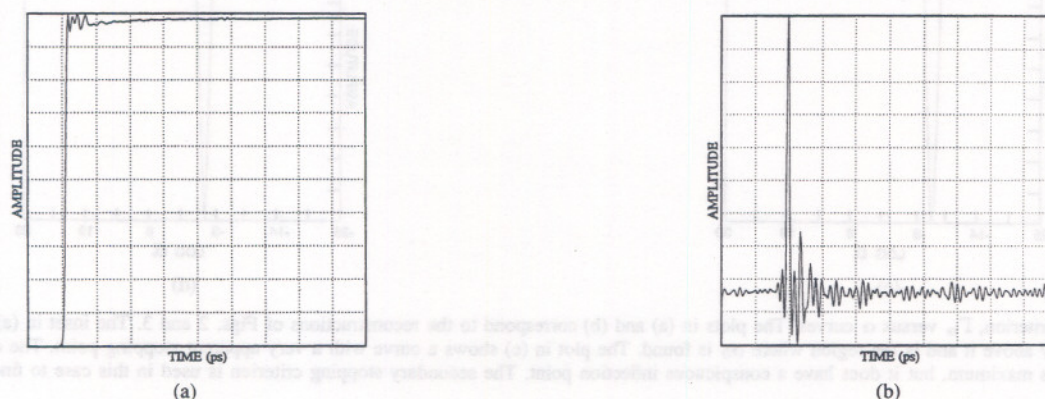

(a)

(b)

Fig. 4.   Reconstruction of an impulse response. The waveform in (a) was deconvolved from that of Fig. 2(a); the result is shown in (b).

B. Reconstruction of Real Waveforms and Stopping Criterion Curves

For illustration, two iterative reconstruction results for real data are shown, one each in Figs. 3 and 4. The figures also include plots of the deconvolution inputs. Fig. 5 shows the Γ_{α}-vs-α curves for the reconstructions presented in Figs. 3 and 4 and for two other reconstructions. These curves can be viewed as displaying the solutions' stability with respect to changes in α; the slope of these curves corresponds to an acceleration. The far left and far right regions of each Γ_{α} versus α curve indicate areas of under and over filtering. For a stable solution to the reconstruction, a search for a maximum between the over- and under-filtered regions is performed. However, more than one maximum may exist. If this occurs, the maximum with the greatest expanse (height and width) has been shown to give the best results.

Looking at Fig. 5(d) we see that the Γ_{α}-vs-α curve does not have a maximum similar to the curves in Figs. 5(a)–(c), but instead has an inflection point. However, by taking the derivative of this curve with respect to α, a new curve is obtained which has attributes that can be used as a stopping criterion. In this new curve, a location is selected that has a zero-valued slope and occurs after the location of the global minimum in the Γ_{α} versus α curve. This new point corre-

sponds to a constant acceleration point and is the secondary stopping criterion.

C. Reconstruction-Waveform Pulse Parameter Statistics

The reliability of this iterative reconstruction was checked by performing 59 reconstructions and comparing certain pulse parameters with those of the input pulse. Of the 59 reconstructions, only six required the secondary stopping criterion. Five of these six are nonsensical reconstructions in that the numerator and denominator functions contained data corresponding to the measurement of two different pulses by the same instrument. The search for α_0 was performed in two steps: a coarse search started at $\alpha = 10^{-25}$, stopped at $\alpha = 10^{30}$, and was incrementally multiplied by $10^{0.5}$; a second search started at one-tenth the α found in the coarse search and was incrementally multiplied by $10^{0.05}$. All reconstructions used 150 iterations, 110 iterations for the coarse search and 40 for the second. Each reconstruction took approximately 12 s using a 33-MHz 80486-based personal computer. The technique of Bennia and Riad, in comparison, which is a performance-enhanced Van–Cittert method, requires 250 000 iterations to converge to a "good" solution. [8]

The pulse parameters compared are: overshoot, undershoot, 10–90% rise time, and 20–80% rise time. For the purpose of
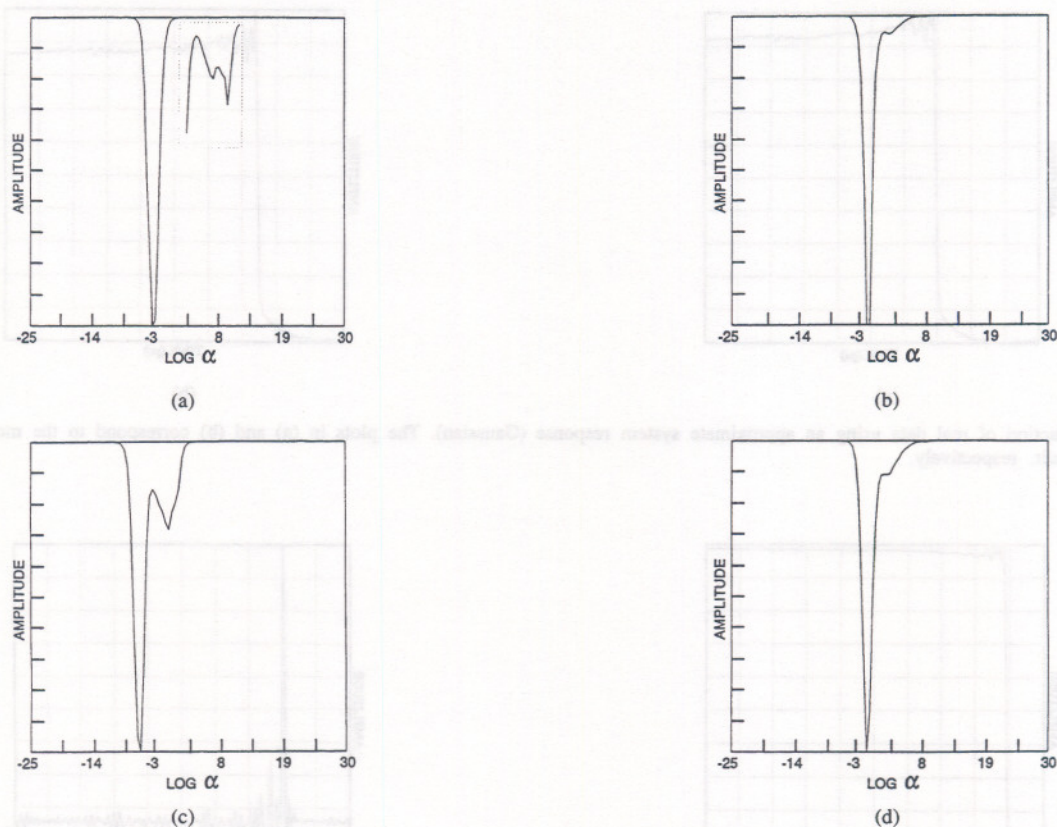
(a)

(b)

(c)

(d)

Fig. 5. Stopping criterion, Γ_α versus α curves. The plots in (a) and (b) correspond to the reconstructions of Figs. 2 and 3. The inset in (a) is an expansion of the curve directly above it and is the region where α_0 is found. The plot in (c) shows a curve with a very apparent stopping point. The curve in (d) does not have an obvious maximum, but it does have a conspicuous inflection point. The secondary stopping criterion is used in this case to find α_0.

this paper these parameters are defined as follows:

(a) overshoot:

$$OS = 100 \left[\frac{g'_{m,\max} - A_{100}}{A_{100} - A_0} \right] \quad (24)$$

(b) undershoot:

$$US = 100 \left[\frac{A_0 - g'_{m,\min}}{A_{100} - A0} \right] \quad (25)$$

and (c) rise time: the time interval between the specified amplitudes.

The pulse parameter comparisons are made by comparing the difference between a reference value and the reconstruction value. For the rise time comparisons, the reference values are obtained from the Gaussian approximation

$$t_r = \sqrt{t_{r,m}^2 - t_{r,s}^2}. \quad (26)$$

The Gaussian approximation provides a good estimate of the reconstruction's rise times (see Table I). For the overshoot and undershoot comparisons, the reference values are the measured data's values because the effect of the instrument on these parameters is difficult to approximate. A distribution of the differences between the reconstructed and reference pulse parameter values illustrates the comparisons; Table I provides statistics of these distributions.

Ringing (undershoot/overshoot) may be observed in g'_m and is caused by deconvolution of data that has steep amplitude transitions [15] and/or discontinuities at the ends of the record.

TABLE I

MEAN, STANDARD DEVIATION, AND RANGE OF THE DIFFERENCES BETWEEN THE RECONSTRUCTION AND REFERENCE PULSE PARAMETERS FOR RECONSTRUCTIONS USING THE REGULARIZING FILTER DESCRIBED HERE (MIDDLE COLUMN) AND A [17] SOLUTION (RIGHT COLUMN)

PULSE PARAMETER DIFFERENCE	$\lvert R_{k,\alpha} \rvert = w_{1,\alpha} R_{1,k} + w_{3,\alpha} R_{3,k}$	Ref. 17
OVERSHOOT (%)		
mean	4.54	5.32
standard deviation	6.24	9.84
range	-1.88 to 13.1	-4.42 to 41.6
UNDERSHOOT (%)		
mean	1.13	3.27
standard deviation	2.46	6.03
range	-0.659 to 15.1	-0.732 to 25.0
RISE TIME (ps) 10%-to-90%		
mean	-0.0714	12.2
standard deviation	7.11	48.9
range	-18.3 to 22.6	-13.3 to 243
RISE TIME (ps) 20%-to-80%		
mean	0.452	4.32
standard deviation	4.12	10.2
range	-3.60 to 16.0	-5.33 to 35.2

The effect of record discontinuities on the reconstructions [25], [26] has been eliminated or minimized. Any ringing observed in the reconstructed data is increased when higher-order difference operators are used, such as those used in some Tikhonov–Miller techniques [17]. Another test for the

proposed algorithm is to set H_k equal to F_k. In this case the algorithm correctly selects the Kroneker-delta as the optimal solution.

The right column shows the statistics using the algorithm described in [17] where the stopping criterion used time-domain errors. In particular, this technique has been implemented using the change in power of the imaginary components of the reconstructed time-domain waveform as a criterion because a correlation between reconstruction appearance and imaginary-component power was more evident than when using the real-component or total power. Consequently, this stopping criterion necessitates the existence of finite-precision arithmetic errors and the use of complex arrays for real-valued inputs to the FFT. That algorithm failed when the positive and negative halves of the spectrum of the iterations were forced to be complex conjugates of each other. The proposed filter and stopping criterion were not affected by these conjugacy errors and functioned using either the entire spectrum or one half. The algorithm of [17] typically provided "good" results though the results contained ringing near steep transitions and occasionally failed to converge to a "good" solution (see Table I).

VI. CONCLUSION

A new regularizing filter and its associated stopping criterion have been described for use in selecting an optimal solution to reconstructions using the blind deconvolution of one transient waveform from another. The filter uses a weighted average of two functions, both of which consist of difference operators and a common variable parameter. The optimal solution is found by varying this parameter until the change in the sum of the magnitudes of the reconstruction's spectral components exhibits a maximum. Convergence of this technique was rapid, approximately 12 s using a 33 MHz 486- based computer. The proposed filter also reduced the ringing observed in reconstructed waveforms that is caused by steep transitions in the measured (input) data. Variations in the pulse parameters, overshoot, undershoot, and rise time were also reduced.

APPENDIX

### Variable List and Description

A_k an approximation to A'_k

A'_k difference between the spectra of the exact (but unknown) and approximate measurement system impulse responses

A_0 baseline amplitude value of waveform

A_{100} topline amplitude value of waveform

D_k spectrum of a difference operator

$d_{m,j}, D_{k,j}$ the jth-order difference operator, its discrete Fourier transform (DFT)

C_α a value used to simplify the selection of the weights of the filters used in the regularizing operator

E_k spectrum of deconvolution error

$E_{k,j}$ difference-operator-dependent errors between different regularized reconstruction spectra

E_α difference between spectra of $R_{1,k}$ and

$R_{3,k}$-regularized reconstructions

$E_{R,k}$ error of regularized reconstruction relative to the ideal reconstruction

f_m, F_k data acquired from the measurement of input signal, its DFT

g_m, G_k discrete representation of the input signal and the ideal solution to the deconvolution, its DFT

g'_m, G'_k regularized stable reconstruction, its DFT

$g'm, \max$ maximum amplitude value of the reconstructed waveform

$g'_{m,\min}$ minimum amplitude value of the reconstructed waveform

$G'\prime_k$ unstable approximation to the deconvolution

H_k spectrum of the approximation to h'_m

h'_m, H'_k impulse response of the measurement instrument, its DFT

k discrete frequency index

m discrete time index

N number of time points over which the data is defined

n_m, N_k additive measurement noise, its DFT

OS   waveform overshoot, time-domain parameter

r_m, R_k the causal regularizing filter, its DFT

$R_{i,k}$ magnitude-only approximations to $R_k; i = 1, 2, 3$

t_r reference rise time

$t_{r,m}$ rise time taken from measurement data

$t_{r,s}$ rise time of the measurement system impulse response

T_k target solution, as explained in text

US   waveform undershoot, time-domain parameter

$w_{1,\alpha}, w_{3,\alpha}$ weights for the two filters, $R_{1,k}$ and $R_{3,k'}$ used in the regularizing filter

Y_α the value from which filter weights are determined

$Y_{\alpha,\lim}$ limiting value of Y, explained in text

$Y_{\alpha,\max}$ maximum attainable value of Y_α

α the adjustable parameter of the regularizing filter

α_0 the value of giving the optimal reconstruction

Γ_α α-dependent change in the spectrum of the reconstruction

δ positive increment in α

θ_k phase of the regularizing function

Γ delay

REFERENCES

[1] T. G. Stockham, Jr., T. M. Cannon and R. B. Ingebretsein, "Blind deconvolution through digital signal processing," *Proc. IEEE*, vol. 63, p. 678, 1975.

[2] S. Kawata and Y. Ichioka, "Iterative image restoration for linearly degraded images. I. Basis," *J. Opt. Soc. Am.*, vol. 70, p. 762, 1980.

[3] Y. Ichioka and N. Nakajima, "Iterative image restoration considering visibility," *J. Opt. Soc. Am.*, vol. 71, p. 983, 1981.

[4] R. G. Lane and R. H. T. Bates, "Automatic multidimensional deconvolution," *J. Opt. Soc. Am. A*, vol. 4, p. 180, 1987.

[5] R. J. Mammone and R. J. Rothacker, "General iterative method of restoring linearly degraded images," *J. Opt. Soc. Am A*, vol. 4, p. 208, 1987.

[6] C. E. Morris, M. A. Richards, and M. H. Hayes, "Iterative deconvolution algorithm with quadratic convergence," *J. Opt. Soc. Am. A*, vol. 4, p. 200, 1987.

[7] R. L. Lagendijk, J. Biemond, and D. E. Boekee, "Identification and restoration of noisy blurred images using the expectation-maximization algorithm," *IEEE Trans. Acoust., Speech, Signal Processing*, vol. 38, p. 1180, 1990.

[8] A. Bennia and S. M. Riad, "Filtering capabilities and convergence of the Van–Cittert deconvolution technique," *IEEE Trans. Instrum. Meas.*, vol. 41, p. 246, 1992.

[9] B. J. Sullivan and H.-C. Chang, "A generalized Landweber iteration for ill-conditioned signal restoration," in *IEEE Int. Conf. Acoustics, Speech and Signal Processing*, Toronto, ON, Canada, May 1991, p. 1729.

[10] T. K. Sarkar, F. I. Tseng, S. M. Rao, S. A. Dianat, and B. Z. Hollmann, "Deconvolution of impulse response from time-limited input and output: Theory and experiment," *IEEE Trans. Instrum. Meas.*, vol. IM-34, p. 541, 1985.

[11] J. B. Abbiss, C. de Mol, and H. S. Dhadwal, "Regularized iterative and non-iterative procedures for object restoration from experimental data," *Optica Acta*, vol. 30, p. 107, 1983.

[12] J. Maeda and K. Murata, "Restoration of band-limited images by an iterative regularized pseudoinverse method," *J. Opt. Soc. Am. A*, vol. 1, p. 28, 1984.

[13] A. Lannes, S. Roques and M. J. Casanove, "Resolution and robustness in image processing: a new regularization principle," *J. Opt. Soc. Am. A*, vol. 4, p. 189, 1987.

[14] W. L. Root, "Ill-posedness and precision in object-field reconstruction problems," *J. Opt. Soc. Am. A*, vol. 4, p. 171, 1987.

[15] R. L. Lagendijk, J. Biemond and D. E. Boekee, "Regularized iterative image restoration with ringing reduction," *IEEE Trans. Acoust. Speech, Signal Processing*, vol. ASSP-36, p. 1874, 1988.

[16] J. P. Noonan and B. Archour, "Iterative minimization of entropic stabilizing functionals in signal restoration," in *IEEE Int. Conf. Acoustics, Speech, and Signal Processing*, Toronto, ON, Canada, May 1991, p. 1737.

[17] N. S. Nahman and M. E. Guillaume, "Deconvolution of time domain waveforms in the presence of noise," National Bureau of Standards Tech. Note 1047, U. S. Department of Commerce, Washington, DC, 1981.

[18] J. Biemond, R. L. Lagendijk, and R. M. Mersereau, "Iterative methods for image deblurring," *Proc. IEEE*, vol. 78 p. 856, 1990.

[19] G. Ross, "Iterative methods in information processing for object restoration," *Optica Acta*, vol. 29, p. 1523, 1982.

[20] A. N. Tikhonov and V. Y. Arsenin, *Solutions of Ill-posed Problems*. Washington, DC: V. H. Winston & Sons, 1977.

[21] A. Bennia and S. M. Riad, "An optimization technique for iterative frequency-domain deconvolution," *IEEE Trans. Instrum. Meas.*, vol. 39, p. 358, 1990.

[22] A. Papoulis, *Signal Analysis*. New York: McGraw-Hill, 1977.

[23] R. E. A. C. Paley and N. Weiner, *Fourier Transforms in the Complex Domain*, American Mathematical Society Colloquium Pub., vol. XIX. New York: American Mathematical Society, 1934.

[24] A. V. Oppenheim and R. W. Schafer, *Discrete-time Signal Processing*. Englewood Cliffs, NJ: Prentice Hall, 1989.

[25] H. F. Silverman and A. E. Pearson, "On deconvolution using the discrete Fourier transform," *IEEE Trans. Audio Electroacoust.*, vol. AU-21, p. 112, 1973.

[26] N. G. Paulter and R. B. Stafford, "Reducing the effects of record truncation discontinuities in waveform reconstructions," *IEEE Trans. Instrum. Meas.*, vol. 42, p. 695, June 1993.
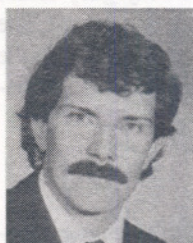
Nicholas G. Paulter, Jr. received the M. S. degrees in chemistry from the University of New Mexico in 1988 and electrical engineering from the University of Colorado in 1990.

He was with Los Alamos National Laboratory, Los Alamos, NM, from 1980 to 1989 and was involved in the study of fast electrical phenomena and the development of high-speed photoconductors for use as ultrafast light detectors and sampling gates. In 1989 he joined the National Institute of Standards and Technology (NIST), Boulder, CO, to develop transient pulse measurement techniques. He is presently with NIST in Gaithersburg, MD. His current research interests include semiconductor physics, electroptics, ultrafast electronic phenomena, and waveform/data processing and analysis.